ISSN 1063-7834, Physics of the Solid State, 2015, Vol. 57, No. 11, pp. 2290–2296. © Pleiades Publishing, Ltd., 2015.
Original Russian Text © S.V. Telegin, S.V. Naumov, O.G. Reznitskikh, E.I. Patrakov, 2015, published in Fizika Tverdogo Tela, 2015, Vol. 57, No. 11, pp. 2222–2227.

PHASE TRANSITIONS

Effect of Cobalt Deficiency on the Structural Phase Transition in $EuBaCo_{2-x}O_{6-\delta}$

S. V. Telegin[a], S. V. Naumov[a,*], O. G. Reznitskikh[b], and E. I. Patrakov[a]

[a] *Mikheev Institute of Metal Physics, Ural Branch of the Russian Academy of Sciences, ul. Sofii Kovalevskoi 18, Yekaterinburg, 620219 Russia*

[b] *Institute of High-Temperature Electrochemistry, Ural Branch of the Russian Academy of Sciences, ul. Sofii Kovalevskoi 22, Yekaterinburg, 620219 Russia*

* *e-mail: naumov@imp.uran.ru*

Received May 12, 2015

Abstract—The effect of cobalt deficiency on the structural phase transition in the double layered cobaltite $EuBaCo_{2-x}O_{6-\delta}$ has been investigated using differential scanning calorimetry and high-temperature X-ray diffraction. It has been shown that, upon introduction of 5% cobalt vacancies, the energy and temperature of the phase transition from the orthorhombic unit cell (space group *Pmmm*) to the tetragonal unit cell (space group *P*4/*mmm*) decrease by 6% and 11°C, respectively, as compared to the corresponding values typical of stoichiometric $EuBaCo_2O_{6-\delta}$. A model of the formation of cobalt–oxygen vacancies has been proposed.

DOI: 10.1134/S1063783415110347

1. INTRODUCTION

Interest in double layered cobaltites of the general formula $LnBaCo_2O_{6-\delta}$ (where *Ln* is a lanthanide) is associated with the following aspects of their consideration: (1) the complex phase diagram, the existence of a number of structural and magnetic transitions, and interesting electrophysical properties [1, 2]; (2) high electrochemical characteristics and the possibility of using compounds of this type as cathodes for intermediate-temperature solid oxide fuel cells (IT-SOFC) [3, 4]. In this regard, double layered cobaltites have been thoroughly studied in recent years. The $LnBaCo_2O_{6-\delta}$ compounds have a layered perovskite-like crystal structure consisting of square layers located along the *c* axis, in which the lanthanide and barium ions are orderly arranged in different planes as follows: [BaO]–[CoO_2]–[$LnO_{6-\delta}$]–[CoO_2]. Owing to the ordering of the *Ln* and Ba ions, the simple cubic perovskite cell with the parameter a_p is doubled along the *c* axis, whereas the ordering of oxygen vacancies results in the ordering along the *b* axis. Therefore, the unit cell corresponds to the formula $a_p \times 2a_p \times 2a_p$ (the "122" phase). At present, the influence of the oxygen content in $LnBaCo_2O_{6-\delta}$ compounds on their properties has been well studied [1, 2, 5, 6]. Moreover, there are a number of studies on the properties of layered cobaltites with different substitutions in the cation sublattice. Substitutions of different 3*d* elements for cobalt are the most thoroughly studied (see, for example, [7, 8]). The cation disorder in systems of the general formula $LnBaCoO_{6-\delta}$ has been studied to a lesser degree. For example, in [9], it was shown that the barium deficiency in the $PrBa_xCo_2O_{6-\delta}$ ($x = 0.94$) compound leads to a change in the thermal expansion coefficient and electrical conductivity with an increase in the number of electron holes, which, in turn, increases the electrochemical characteristics of $PrBa_xCo_2O_{6-\delta}$ cathodes [9].

Our experiments on the growth and study of the properties of $GdBaCo_{2-x}O_{6-\delta}$ single crystals revealed that the growth of single crystals of layered cobaltites using crucibleless melting can be accompanied by the evaporation of cobalt during the melting with the formation of the single-phase structure. The physicochemical properties of $GdBaCo_{2-x}O_{6-\delta}$ single crystals differ from those typical of cobalt-stoichiometric samples [10–12]. We assume that the functional properties of $LnBaCo_{2-x}O_{6-\delta}$ compounds can be purposefully changed by varying the cobalt concentration. The experiments on polycrystalline samples and $GdBaCo_{2-x}O_{6-\delta}$ single crystals [10, 11], as well as the preliminary analysis of the data for the $EuBaCo_{2-x}O_{6-\delta}$ system demonstrated that the structural phase transition *Pmmm* → *P*4/*mmm* at $T \sim 450$°C is the most sensitive to vacancies in the cobalt sublattice. This phase transition is caused by the loss of oxygen during heating and by a uniform distribution of oxygen ions between the [CoO_5] pyramids with the $V_O^{\bullet\bullet}$ vacancy in the O4 position and the [CoO_6] octahedra with the oxygen ions O_O^X in the O3 position. This leads to a disordering along the *b* axis, and the orthorhombic space

group *Pmmm* transforms into the tetragonal space group *P*4/*mmm*. The most detailed and systematic investigations of this phase transition were performed in [13, 14]. In [13], it was shown that the phase transition *Pmmm* → *P*4/*mmm* is a first-order phase transition and can affect the mechanism of electrical conduction at high temperatures, i.e., in the temperature range where double cobaltites are assumed to be used as cathodes of solid oxide fuel cells.

The object of investigation was chosen to be the $EuBaCo_{2-x}O_{6-\delta}$ ($x = 0, 0.1$) system. The choice of the $EuBaCo_{1.9}O_{6-\delta}$ composition was determined by our preliminary experiments [9], according to which the phase boundary of the existence of the double perovskite does not exceed the concentration $x \sim 0.1$. The purpose of this work was to investigate the effect of cobalt deficiency on the structural phase transition *Pmmm* → *P*4/*mmm* in $EuBaCo_{2-x}O_{6-\delta}$ ($x = 0, 0.1$) samples at temperatures ranging from 400 to 500°C.

2. SAMPLE PREPARATION AND EXPERIMENTAL TECHNIQUE

Polycrystalline samples of $EuBaCo_{2-x}O_{6-\delta}$ cobaltites were synthesized using the Pechini method [15]. The initial components were Eu_2O_3, $BaCO_3$, and Co. The reactants were preliminarily calcined (Eu_2O_3, 900°C), dried ($BaCO_3$, 500°C), and reduced in a hydrogen flow (Co, 600°C). The initial components are dissolved in a dilute nitric acid. Then, an equimolar solution of citric acid (CA) and ethylene glycol (EG) was added in a ratio of 3 (CA and EG) : 1 metal ion. The obtained mixture was heated to 80°C with continuous stirring to polymerization with the formation of a viscous material. This material was heated in a furnace first at 140°C for 4 h to the formation of an amorphous polymer and then to 250°C for 2 h to charring of the formed polymer rubber.

Then, the samples were subjected to stepwise annealing in the temperature range from 900 to 1150°C with the intermediate dispersion. After completion of the synthesis, all the samples were slowly cooled with the furnace (at a rate of 1°C/min). The phase composition and crystal structure of the samples at room temperature and in the range from 450 to 500°C were determined on a DRON-3 diffractometer (CuK_α radiation) equipped with a high-temperature attachment. The heating and cooling of the sample during the temperature investigations were performed at a rate of 50°C/h. The sample was exposed to each temperature of measurement until the diffraction pattern remained unchanged with time. The recording was performed first during heating and then during cooling of the sample in order to check the reproducibility of the obtained data. The calculations of the crystal structure and the refinement of the structural parameters from the results of the X-ray diffraction analysis were performed with the PowderCell 2.3 software package [16]. The elemental analysis of the samples was carried out on an FEI Inspect F scanning electron microscope with an EDAX energy-dispersive X-ray spectrometer. The absolute oxygen content in the studied samples was determined using the method of hydrogen reduction to initial oxides (Eu_2O_3, BaO) and metallic cobalt. The thermal analysis, which made it possible to investigate the sample simultaneously using differential scanning calorimetry (DSC) and thermogravimetry (TG), was performed on a Netzsch STA 409 F1 Jupiter thermal analyzer in an air flow at a temperature in the range from 30 to 600°C during heating and cooling at a rate of 5°C/min.

3. EXPERIMENTAL RESULTS

We synthesized polycrystalline samples of $EuBaCo_{2-x}O_{6-\delta}$ ($x = 0, 0.1$) cobaltites. The elemental analysis demonstrated that the cation composition of the samples is close to the nominal composition. The $EuBaCo_{2-x}O_{6-\delta}$ samples with $x = 0$ and 0.1 at room temperature have the oxygen nonstoichiometry indices $\delta = 0.50 \pm 0.02$ and 0.65 ± 0.02, respectively. As a result, the average degree of oxidation of cobalt ions Co^{3+} in the cobalt-deficient samples is equal to that of the cobalt-stoichiometric samples synthesized under the same conditions. Figure 1 shows fragments of the X-ray diffraction patterns measured for polycrystalline samples of the $EuBaCo_2O_{5.50}$ and $EuBaCo_{1.9}O_{5.35}$ cobaltites at room temperature. The synthesized samples have a single-phase structure with the orthorhombic space group *Pmmm*. The unit cell parameters are presented in Table 1. It can be seen from this table that, with an increase in the cobalt deficiency, the unit cell parameter *c* changes most significantly, and the unit cell volume increases. Fragments of the DSC and

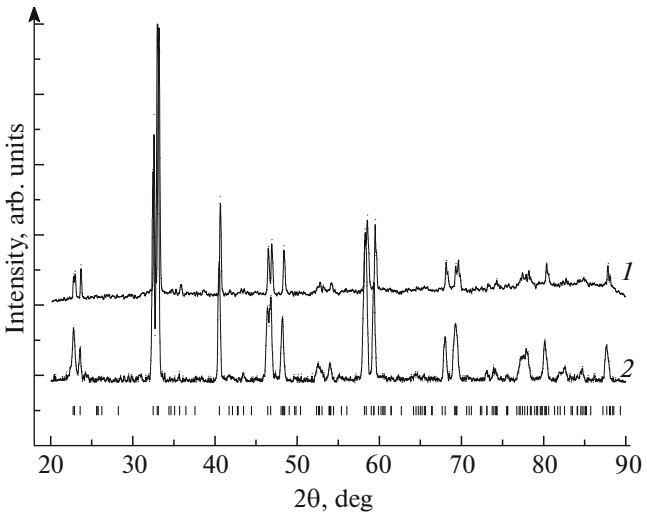

Fig. 1. Fragments of the X-ray diffraction patterns of (*1*) $EuBaCo_2O_{5.50}$ and (*2*) $EuBaCo_{1.9}O_{5.35}$. Vertical bars indicate the positions of the peaks.

Table 1. Unit cell parameters and the unit cell volume of the $EuBaCo_{1.9}O_{5.35}$ and $EuBaCo_2O_{5.50}$ samples at room temperature

Composition	a, Å (±0.001)	b, Å (±0.002)	c, Å (±0.002)	V, Å^3
$EuBaCo_2O_{5.50}$	3.881	7.827	7.536	228.96
$EuBaCo_{1.9}O_{5.35}$	3.884	7.826	7.551	229.52

TG curves of the $EuBaCo_2O_{6-\delta}$ and $EuBaCo_{1.9}O_{6-\delta}$ samples in the temperature range from 50 to 600°C are shown in Fig. 2. The DSC curve for the $EuBaCo_2O_{5.50}$ sample is typical of double cobaltites [17]: the heating and cooling curves are characterized by pronounced thermal effects with maxima at $T \sim 80$ and ~460°C, respectively, which correspond to two well-known phase transitions. The low-temperature phase transition is accompanied by a sharp and anisotropic change in the unit cell parameters, whereas the symmetry of the lattice remains orthorhombic. The high-temperature phase transition, as was noted above, is associated with the redistribution of oxygen ions between the positions O3 and O4 [14], as well as with the change in the symmetry of the unit cell from orthorhombic (space group *Pmmm*) to tetragonal (*P*4/*mmm*) [13, 14, 17].

As can be seen from Fig. 2, the peak in the DSC curve of the sample with a cobalt deficiency, which corresponds to the high-temperature thermal effect, has a complex shape. Noteworthy is a good reproducibility of the DSC curves: all the peaks observed in the heating curves are retained in the cooling curves with the opposite sign of the thermal effect. Let us consider in more detail the DSC curve in the temperature range near the phase transition $Pmmm \rightarrow P4/mmm$. Figure 3 shows fragments of the DSC curves in the temperature range from 420 to 500°C. The temperature of the onset of the phase transition upon heating is equal to 466°C for $EuBaCo_2O_{6-\delta}$ (at $\delta = 0.55$) and 455°C for $EuBaCo_{1.9}O_{6-\delta}$ (at $\delta = 0.70$), which corresponds to an approximately 10°C shift of the phase transition observed in the high-temperature X-ray diffraction patterns. As can be seen from Fig. 4, the structural transformation of the $EuBaCo_2O_{6-\delta}$ sample occurs in the temperature range from 460 to 470°C, unlike $EuBaCo_{1.9}O_{6-\delta}$ in which the phase transition is observed at $T \sim 450$–460°C (Fig. 4 and Table 2). According to the DSC data, the temperatures of the

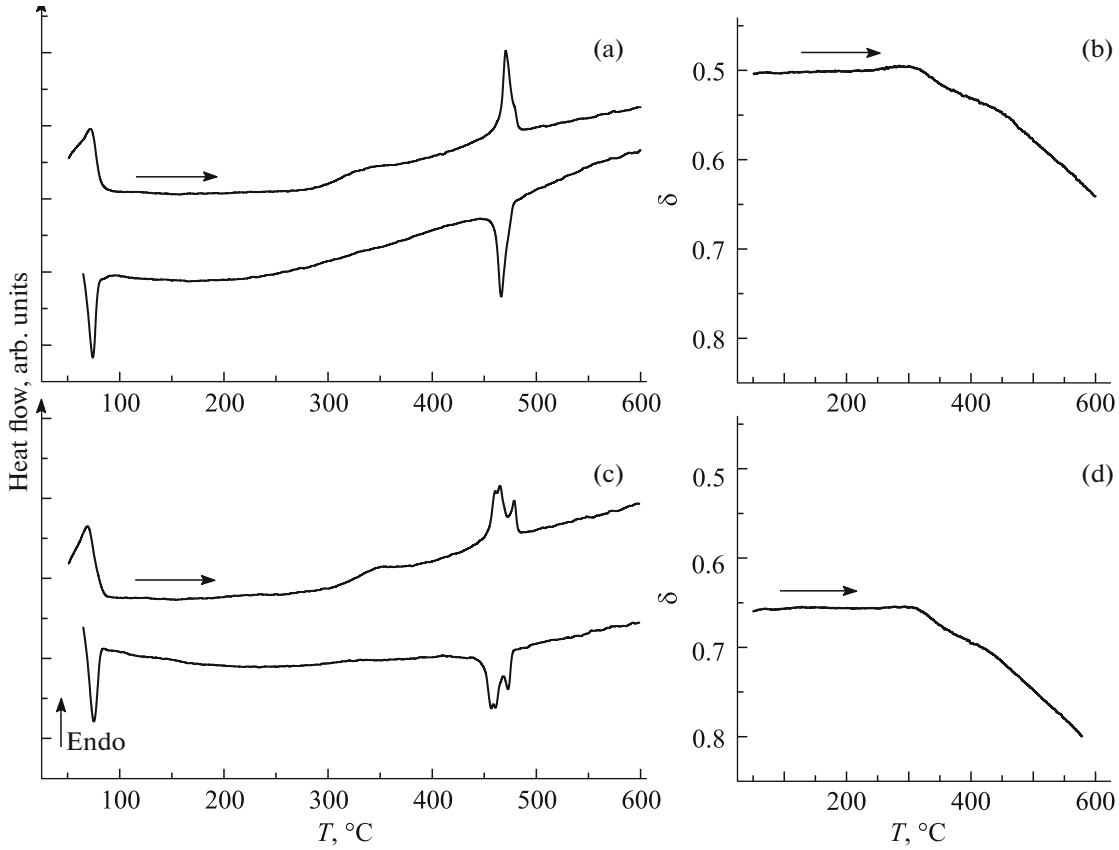

Fig. 2. (a, c) Fragments of the DSC curves and (b, d) temperature dependences of the oxygen nonstoichiometry index δ for (a, b) $EuBaCo_2O_{6-\delta}$ and (c, d) $EuBaCo_{1.9}O_{6-\delta}$. Arrows indicate the heating curves.

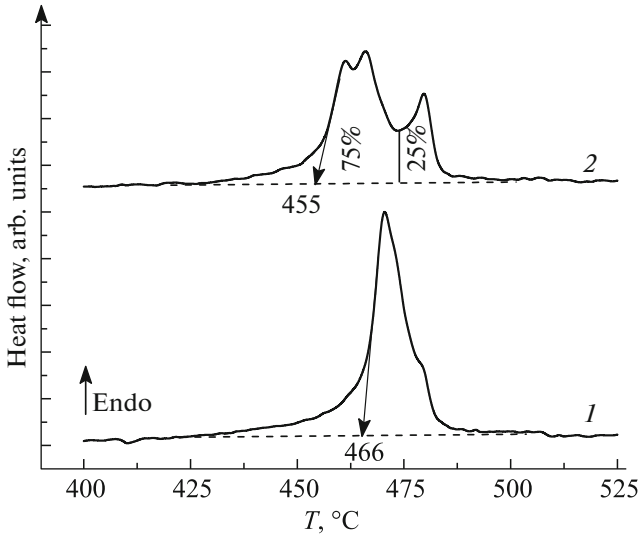

Fig. 3. Fragments of the DSC heating curve in the temperature range from 420 to 500°C for (*1*) $EuBaCo_2O_{6-\delta}$ and (*2*) $EuBaCo_{1.9}O_{6-\delta}$. Arrows indicate the temperatures of the onset of the phase transitions. The separation of the area under curve *2* by 75 and 25% is shown.

reverse phase transition $P4/mmm \rightarrow Pmmm$ upon cooling of the samples are identical and equal to 479°C.

The peak in the DSC curve, which corresponds to the phase transition in $EuBaCo_{1.9}O_{6-\delta}$, is transformed into a triplet with maxima at 461, 466, and 480°C. Taking into account the shape of the peak and the proximity of the maxima, we ignored the separation of the peaks at 461 and 466°C for the $EuBaCo_{1.9}O_{6-\delta}$ sample. As a result, there are two characteristic peaks, one of which contributes 75% of the total energy of the phase transition, and, correspondingly, the contribution of the other peak is 25% (Fig. 3). As follows from Table 2, the energy of the phase transition $Pmmm \rightarrow P4/mmm$ for the $EuBaCo_{1.9}O_{6-\delta}$ compound is approximately 6% less than that for the $EuBaCo_2O_{6-\delta}$ compound.

Table 2. Energies E and temperatures T_{PT} of the phase transition $Pmmm \rightarrow P4/mmm$ according to the data of differential scanning calorimetry (DSC) and X-ray diffraction (XRD) for $EuBaCo_2O_{5.5}$ and $EuBaCo_{1.9}O_{5.35}$ (the oxygen nonstoichiometry index δ is given for the temperatures of the onset of the phase transition).

Composition	E, J/g	T_{PT}, °C		δ
		DSC	XRD	
$EuBaCo_2O_{6-\delta}$	3.6	466	460–470	0.55
$EuBaCo_{1.9}O_{6-\delta}$	3.4	455	450–460	0.70

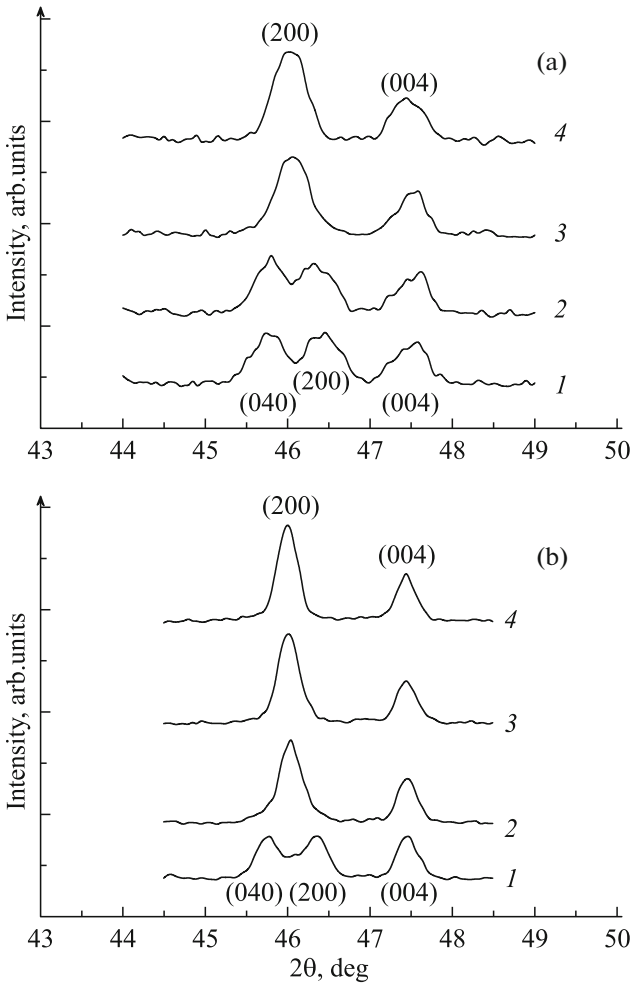

Fig. 4. Fragments of the X-ray diffraction patterns of (a) $EuBaCo_2O_{6-\delta}$ and (b) $EuBaCo_{1.9}O_{6-\delta}$ at temperatures $T =$ (*1*) 450, (*2*) 460, (*3*) 470, and (*4*) 500°C.

4. DISCUSSION OF THE RESULTS

The phase transition $Pmmm \rightarrow P4/mmm$ in the cobalt-deficient $EuBaCo_{2-x}O_{6-\delta}$ samples has a more complex character as compared to the stoichiometric $EuBaCo_2O_{6-\delta}$ compounds.

Let us consider a model system consisting of 100 unit cells (the scheme of one unit cell in the *bc* plane is shown in Fig. 5a) of $EuBaCo_2O_{5.50}$ (*Pmmm*, $Z = 2$). This system contains 400 cobalt ions (Co_{Co}^{X}), 100 oxygen ions (O_{O}^{X}) in the O3 positions, and 100 unoccupied positions O4. The heating to the phase transition temperature leads to a partial escape of the oxygen ions from the O3 positions. According to the thermogravimetry data, the model system loses ten oxygen ions from the O3 positions and retains 90 occupied positions O3. As was shown in [14], the phase transition is accompanied by a uniform distribu-

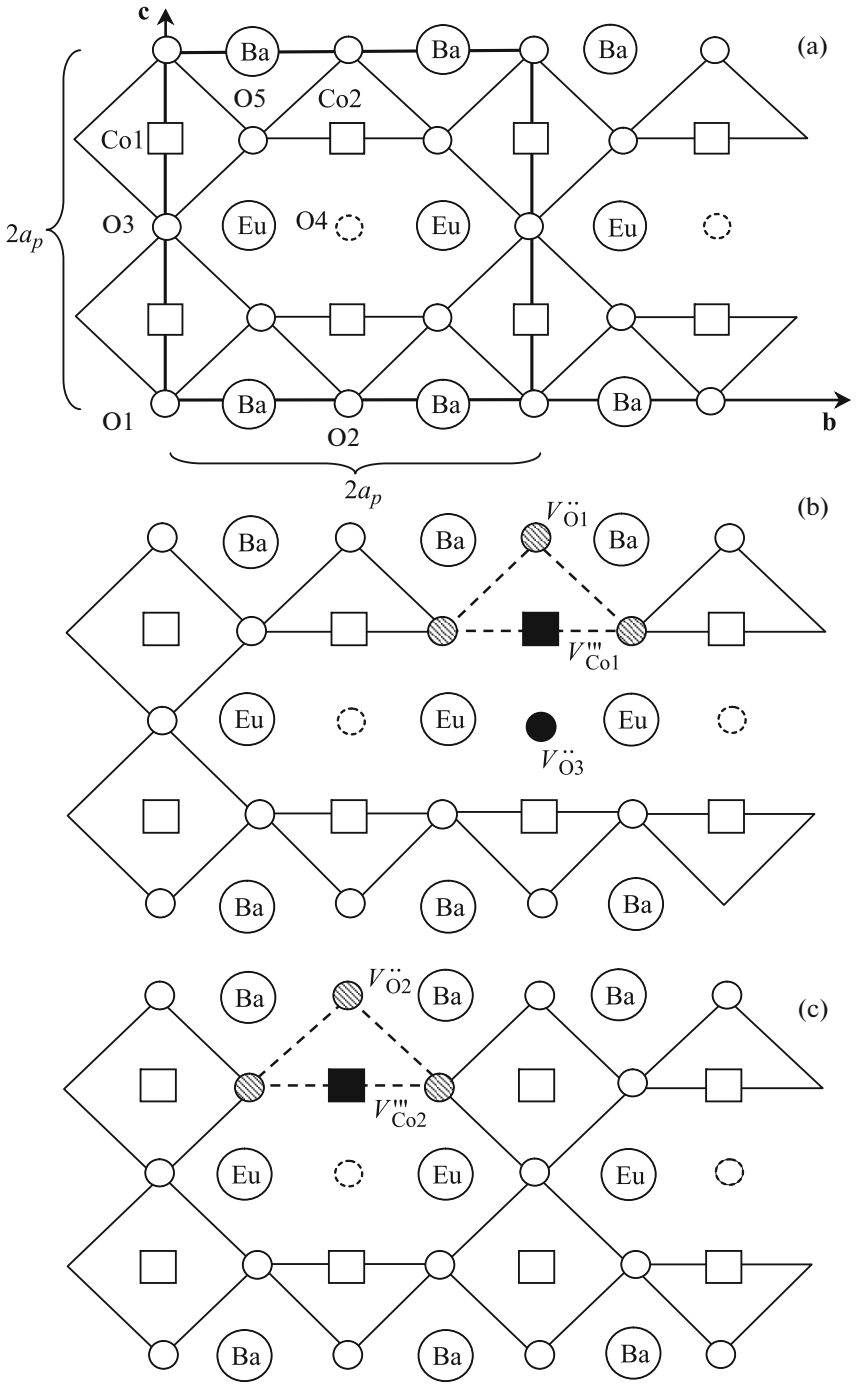

Fig. 5. Schematic diagrams of the formation of cobalt–oxygen vacancies in the *bc* plane: (a) $EuBaCo_2O_{5.50}$ unit cell (all the O4 positions are unoccupied, and all the O3 positions are occupied by oxygen ions), (b) model system where the cobalt vacancy is located in the Co1 ($V_{Co1}^{'''}$) position, and (c) model system where the vacancy cobalt is located in the Co2 ($V_{Co2}^{'''}$) position. The shaded oxygen positions are possible sites of the formation of oxygen vacancies. The positions designated as $V_{O1}^{\bullet\bullet}$, $V_{O2}^{\bullet\bullet}$, and $V_{O3}^{\bullet\bullet}$ are the most preferred sites of the formation of oxygen vacancies bound to the cobalt vacancy.

tion of oxygen ions between the positions O3 and O4. Thus, among the 90 oxygen ions in the O3 positions, the 45 ions are displaced to the O4 positions, whereas the other 45 ions remain in the O3 positions.

Now, we introduce cobalt vacancies into the model system (Figs. 5b, 5c). We assume that the cobalt vacancies are uniformly distributed between the positions Co1 and Co2, while their related additional oxy-

gen vacancies are located in the nearest positions. In our opinion, the formation of vacancies most probably occurs in the following positions: a vacancy in the position of the mobile oxygen O3 and vacancies in the positions O1 and O2. The latter assumption is based on the close values of the O3–Eu–O4 and O1–Ba–O2 bond lengths (Fig. 5).

Thus, the introduction of 5% cobalt vacancies into our model system leads to the formation of $10V_{Co1}^{'''}$ and $10V_{Co2}^{'''}$ (cobalt vacancies in the positions Co1 and Co2, respectively) and $10V_{O1}^{\bullet\bullet}$, $10V_{O2}^{\bullet\bullet}$, and $10V_{O3}^{\bullet\bullet}$ (oxygen vacancies in the corresponding positions). In this case, 380 cobalt ions (Co_{Co1}^{X} and Co_{Co2}^{X}) and 90 oxygen ions O3 remain in their initial positions. The heating to the phase transition temperature, as was described above, leads to a partial escape of oxygen ions from the O3 positions. At this temperature in the cobalt-deficient model system, 80 oxygen ions remain in the O3 positions, of which 40 ions execute jumps into the O4 positions and the other 40 ions remain in their positions.

Since the thermal effect of the phase transition, which is visible in the DSC curve, represents the total energy of all the jumps made by the oxygen ions O3 → O4 and their influence on the unit cell, the introduction of 5% cobalt vacancies leads to a decrease in the number of jumps O3 → O4 from 45 for the model system $EuBaCo_2O_{6-\delta}$ to 40 for $EuBaCo_{1.9}O_{6-\delta}$. Therefore, the difference in the energies of the phase transitions between the cobalt-stoichiometric sample and the sample with vacancies should be $\Delta E_{calc} = (45–40)/45 \times 100\% = 11\%$, whereas the experimental value is $E_{exp} \approx 6\%$. Based on the value of E_{calc} obtained from simple quantitative evaluations, we believe that our model of the formation of cobalt–oxygen vacancies satisfactorily describes the actual processes. When comparing E_{calc} and E_{exp}, it is necessary to take into account that we considered, as the basis, the ideal unit cell of the $EuBaCo_2O_{5.5}$ compound without regard for the partial filling of the oxygen positions O4 [14].

As a result, based on the assumption of a uniform distribution of cobalt vacancies between the Co1 and Co2 positions, we obtained a model system in which

(i) the oxygen nonstoichiometry index δ coincides with the experimental value: two cobalt vacancies lead to the formation of three additional oxygen vacancies;

(ii) the change in the energy of the phase transition in the presence of 5% cobalt vacancies is $E_{calc} = 11\%$.

At the same time, one cobalt vacancy in the O3 position has a significant effect on the nearest environment. This is indicated by the formation of a triplet and the area ratio of the DSC peaks for the $EuBaCo_{1.9}O_{5.35}$ sample. It can be assumed that the DSC peaks at temperatures of 461–466°C correspond to the phase transitions of the unit cells under the influence of cobalt–oxygen vacancies. Moreover, for unit cells not affected by the vacancies, the phase transition manifests itself in the DSC curve as a peak with the maximum at 470°C (the temperatures of the onset of the phase transition upon cooling coincide for both samples). In this case, it turns out that 5% vacancies in the cobalt sublattice affect the state of ~3/4 of the entire system of cobalt–oxygen bonds involved in the formation of the structural phase transition (Fig. 3). This means that a region of structural distortions or a cluster consisting of several unit cells is formed around one unit cell containing a cobalt vacancy. We can estimate the cluster sizes. According to our assumptions about the mechanism of the formation of vacancies, 5% cobalt vacancies lead to the formation of 10% oxygen vacancies in the O3 positions. If it is assumed that the environment of these cells is responsible for the 75% contribution to the phase transition energy, the vacancy has an effect on 7–8 unit cells, which are the nearest neighbors. Then, it turns out that the cluster size corresponds to the structural formula ~$3a \times 3b \times 3c$. These cells are distorted predominantly along the c axis, have a larger volume, and undergo a phase transition at a lower temperature (Table 2). It can also be assumed that the existence of these clusters will have an effect not only on the DSC curves but also on other properties depending on the state of the cobalt ion or on the energy of cobalt–oxygen bonds.

ACKNOWLEDGMENTS

We would like to thank Yu.E. Turkhan for his assistance in performing the high-temperature X-ray diffraction analysis.

The study was supported by the Federal Agency of Scientific Organizations (FASO) of Russia within the framework of the state task on the theme "Spin" (no. 01201463330) and, in part, by the Russian Foundation for Basic Research (project no. 14-02-00432) and the Ural Branch of the Russian Academy of Sciences (project no. 15-9-2-4).

REFERENCES

1. A. A. Taskin, A. N. Lavrov, and Y. Ando, Phys. Rev. B: Condens. Matter **71**, 134414 (2005).
2. C. Frontera, J. L. Garcĭa-Muňoz, A. Llobet, and M. A. G. Aranda, Phys. Rev. B: Condens. Matter **65**, 180405 (2002).
3. A. J. Jacobson, Chem. Mater. **22**, 660 (2010).
4. S. Ya. Istomin and E. V. Antipov, Usp. Khim. **82**, 686 (2013).
5. A. A. Taskin, A. N. Lavrov, and Y. Ando, Appl. Phys. Lett. **86**, 091910 (2005).
6. D. S. Tsvetkov, V. V. Sereda, and A. Yu. Zuev, Solid State Ionics **180**, 1620 (2010).
7. Y.-K. Tang and C. C. Almasan, Phys. Rev. B: Condens. Matter **77**, 094403 (2008).

8. B. Raveau, Ch. Simon, V. Caignaert, V. Pralong, and F. X. Lefevre, J. Phys.: Condens. Matter **18**, 10237 (2006).
9. J. Wang, F. Meng, T. Xia, Z. Shi, J. Lian, C. Xu, H. Zhao, J.-M. Bassat, and J.-C. Grenier, Int. J. Hydrogen Energy **39**, 18392 (2014).
10. S. V. Naumov, S. V. Telegin, D. S. Tsvetkov, E. I. Patrakov, O. G. Reznitskikh, and V. S. Gaviko, Izv. Akad. Nauk, Ser. Fiz. **77**, 1513 (2013).
11. T. I. Arbuzova, S. V. Telegin, S. V. Naumov, E. I. Patrakov, and O. G. Reznitskih, Solid State Phenom. **215**, 83 (2014).
12. L. V. Nomerovannaya, A. A. Makhnev, S. V. Naumov, and S. V. Telegin, Phys. Solid State **57** (4), 776 (2015).
13. L. Mogni, F. Prado, C. Jimenez, and A. Caneiro, Solid State Ionics **240**, 19 (2013).
14. S. Streule, A. Podlesnyak, D. Sheptyakov, E. Pomjakushina, M. Stingaciu, K. Conder, M. Medarde, M. V. Patrakeev, I. A. Leonidov, V. L. Kozhevnikov, and J. Mesot, Phys. Rev. B: Condens. Matter **73**, 094203 (2006).
15. M. P. Pechini, US Patent 3330697 (1967).
16. W. Kraus and G. Nolze, J. Appl. Crystallogr. **9**, 301 (1996).
17. A. Tarancón, D. Marrero-López, J. Peña-Martinez, J. C. Ruiz-Morales, and P. Núñez, Solid State Ionics **179**, 611 (2008).

Translated by O. Borovik-Romanova